J. Fluid Mech. (1974), *vol.* 62, *part* 4, *pp.* 625–642
Printed in Great Britain

Phase and amplitude discrepancies in the surface wave due to a wedge-ended hull form

By R. G. STANDING
Ship Division, National Physical Laboratory

(Received 20 June 1973)

A deep surface-piercing wedge-ended hull model was towed through still water. Measurements of the surface wave pattern confirmed earlier findings for ship models, that the measured bow-wave cusp line often lies well forward of the position predicted by thin-ship theory, and that this shift increases with bow water-line angle and with decreasing model speed. Two possible explanations are considered here in terms of changes of wave phase speed with wave convection and steepness. Calculations based on a transformation method due to Guilloton predict more realistic wave profiles than linear theory, but account for less than half the observed shift. Some tentative conclusions are drawn.

The singularity in the Green's function double integral is removed by an improved method, which simplifies the numerical integration. The new integrand decays within one oscillation.

1. Introduction

The wave-making properties of ships, in particular the wave-making resistance, are often calculated using linear theory. Although these predictions agree fairly well with experiment, there seem to be certain consistent differences, which hinder attempts to interpret the measured far-field pattern and improve hull design methods. In 1909 Hovgaard described how the wave crests tend to lie outboard of the linear wave pattern, the outward shift depending on both craft speed and bow water-line angle. Linear theory predicts the wave pattern quite well when fine-formed craft travel at moderate speeds. The discrepancies increase with craft fullness and bow water-line angle (Shearer 1951; Everest & Hogben 1970; Mori, Inui & Kajitani 1972), especially at moderate and small beam and draught Froude numbers (Everest & Hogben 1970; Dagan 1972), and possibly at large length Froude numbers (Hogben 1971). Other authors who mentioned these discrepancies include Wigley (1931), Hogben (1957), Inui (1962) and Gadd (1969, 1971, 1973).

Several authors tried to explain the discrepancies in terms of second-order wave perturbations. Eggers (1970) improved his predictions of wave-making resistance by including second-order corrections. But it is hard to see how second-order effects can account for the observed outward shift of the bow wave. Eggers identified the second-order perturbations with wave-making sources and doublets distributed over the hull and free surface. According to Lamb (1932)

and Ursell (1960) the linear wave making of a Kelvin source is small outside a critical line making an angle of 19° 28′ with its line of travel. Wave pattern measurements, however, often show wave cusps well outside the critical line for a source at the craft bow. Provided that no part of the hull surface lies outside this angle, sources on the hull surface are unlikely to cause these disturbances. As for the second-order free-surface sources, their density depends on the local linear wave velocity components and their derivatives. Outside the critical line for a bow source these components too are small, so that the free-surface sources are unlikely to cause much wave making. Yim (1964) calculated a single term of the second-order solution, a line integral involving sources along the water-line and representing the most important second-order term for a shallow-draught vessel. He predicted a forward shift of the far-field waves behind the craft, but the above argument suggests that a large bow wave shift can be discounted. Unfortunately Yim presented no comparable experimental results nor calculations close to the craft.

The bow wave shift seems to arise from nonlinearities in the free-surface condition. Lighthill, in the discussion of Gadd's (1969) paper, proposed that small nonlinear variations of the phase velocity may cause large changes of wave shape in the far field, which perturbation procedures cannot accurately predict. A similar problem arises when locating shock waves in supersonic flows (Van Dyke 1964, chap. 6). Two different nonlinear processes seem to be involved. In the first, a process suggested by Gadd (1969) and enlarged on by Lighthill, the phase velocity increases as the waves become steeper. Thus in two dimensions the third-order, regular, free-wave speed c is related to the amplitude a and wavenumber k by

$$c^2 = (g/k)\,(1 + k^2a^2),$$

where g is the acceleration due to gravity. Hogben (1972*a*) obtained a similar third-order perturbation solution describing the free-wave contribution to the wave making of a single source moving along a channel. He concluded that, when the waves are realistically steep, the resulting phase velocity changes cannot account for measured phase shifts. A rough calculation for the double-wedge model, in § 6, confirms Hogben's conclusion. Hogben suggested that local terms may steepen the wave enough to cause a phase shift in the near field. A complete third-order solution is required, but this is out of the question at present. Newman (1971) expressed some doubt about the stability of such a solution near the critical line.

In the second nonlinear process, suggested first by Hovgaard (1909) and later by Gadd (1971), the waves are convected outwards as the mean flow is deflected around the hull. Dagan (1972) showed that the usual linear thin-ship solution is invalid at low speeds, when the transverse wavelength is comparable with the craft beam. To find a wave solution uniformly valid at low speeds he used a varying, rather than uniform, basic velocity distribution in the free-surface boundary condition. Using a different approach Gadd (1971) described the wave convection effect by distorting a linear pattern, and thus substantially improved predictions of hull wave profiles. Guilloton's (1964) transformation method involves a similar distortion. His empirical approach may have something

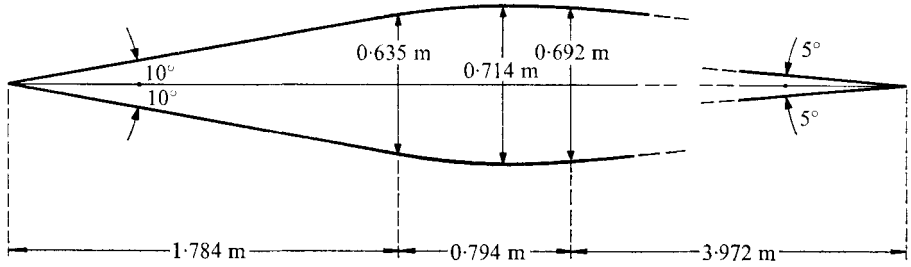

FIGURE 1. The double-wedge model in plan view.

in common with Lighthill's method of strained co-ordinates, described by Van Dyke (1964, chap 6). Gadd (1973) used Guilloton's method to predict the wave making of various ship forms, and largely eliminated phase and amplitude discrepancies between measured and calculated wave profiles and in the wave-making resistance.

Wigley (1931) and Shearer (1951) measured wave profiles along the sides of mathematical models, and Hogben (1957), Inui (1962) and Gadd (1969, 1971, 1973) made similar measurements with more realistic ship models. Japanese authors including Inui (1962), Kajitani (1963) and Mori *et al.* (1972) assembled contour maps of wave heights around ship-shaped models. A simple model was adopted in this paper to reduce the number of quantities affecting the wave pattern. The model consisted of two deep wedges, joined back-to-back around a curved mid-section. Thus the effects of bow water-line angle and craft speed were examined as far as possible in isolation. Detailed contour maps of the wave surface near the bow show how the far-field phase shifts developed when the model was driven in each direction at two speeds. Experimental results are compared with linear theory in §4 and with the results of applying Guilloton's transformation method in §5.

2. Experiments

Figure 1 shows in plan view the model which set up the wave patterns. It consisted of two wedges with vertical faces, joined back-to-back around a curved mid-section. The two wedge half-angles of 5° and 10° were chosen on the basis of earlier experiments (Shearer 1951; Everest & Hogben 1970). These suggested that running the model with its fine end forward should give a small but measurable phase shift, while running with the blunt end forward should give a more marked phase shift, but without the complications of breaking waves. The model speeds, nominally 1·22 and 1·83 m/s, were large enough to allow wave heights to be measured with reasonable accuracy, while admitting at least one transverse wavelength between the bow and the shoulder. The model draught of 0·73 m was effectively infinite at both speeds for the free-wave component of the linear wave pattern. But the model was not deep enough to make the local component independent of draught, and the model cannot be regarded as truly two-dimensional, especially at the higher speed.

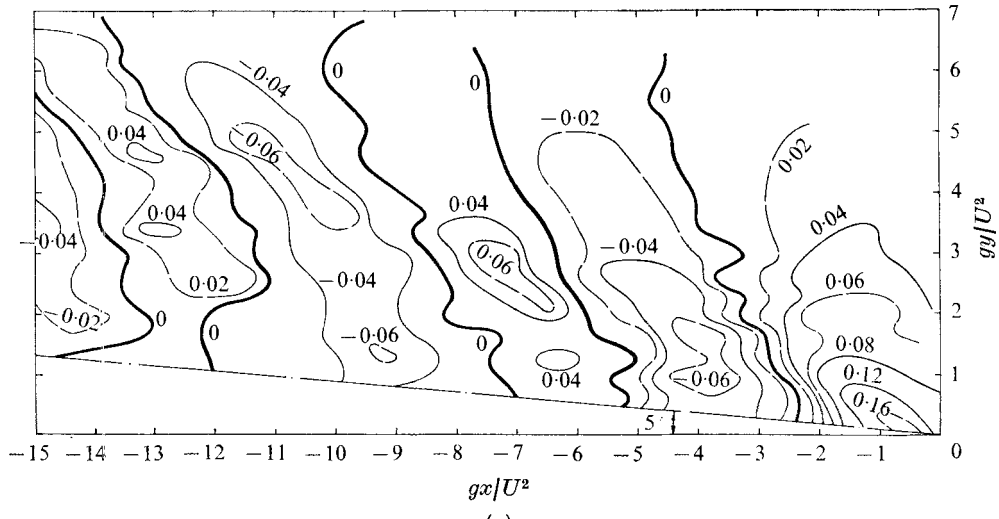

(*a*)

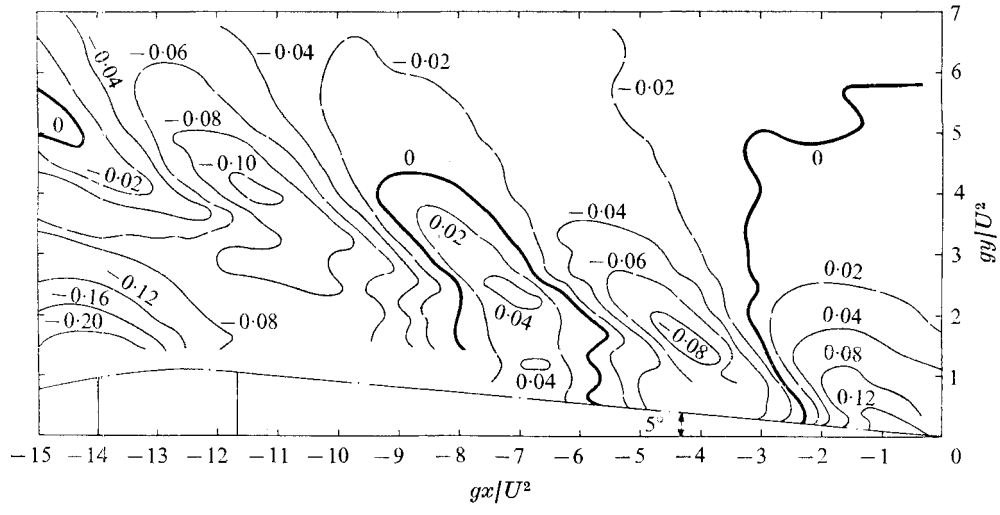

(*b*)

FIGURES 2(*a*, *b*). For legend see facing page.

The tests were carried out at NPL in no. 2 tank, the water depth being 2·74 m and the tank width 6·10 m. The model was driven past Hogben's (1972*b*) automated wave height probes, which were placed at distances 0·65, 1·24 and 1·81 m from the tank centre-line. The probe outputs were recorded digitally on paper tape for subsequent computer analysis. By repeating runs with the model fixed at various distances from the tank centre-line, wave profiles were obtained along longitudinal cuts through the steady pattern 0·038 m apart. Overlapping areas of wave pattern from adjacent probes matched well, suggesting that tank wall effects were negligible ahead of the wave reflexion. Tank bottom effects were also negligible. A manually set comb of pointers measured the bow wave pattern close to the model. The comb was moved across in steps which gave longitudinal

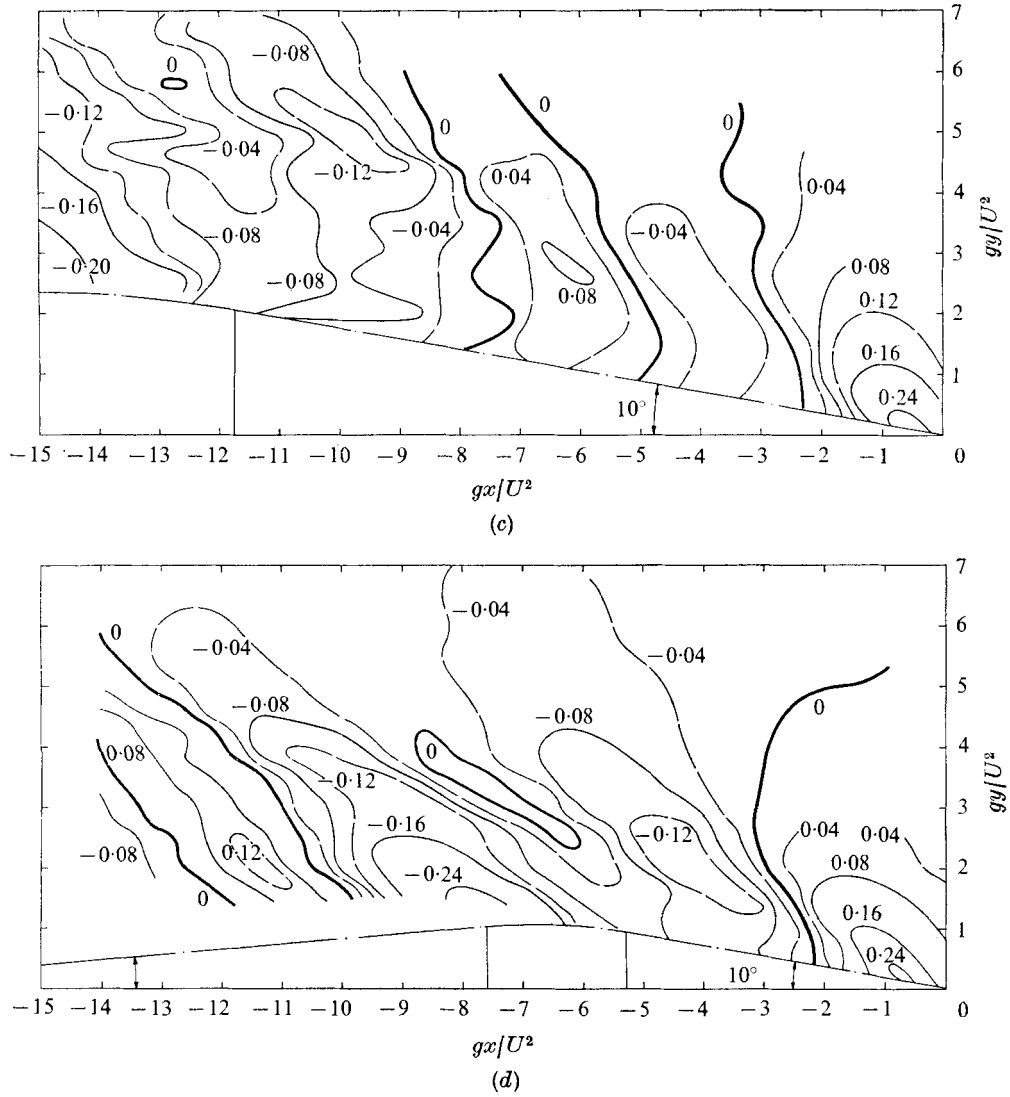

FIGURE 2. Contour maps of measured wave height $g\zeta/U^2$. The numbers indicate the dimensionless contour heights. Fine bow: (*a*) $U = 1{\cdot}22$ m/s, (*b*) $U = 1{\cdot}83$ m/s. Blunt bow: (*c*) $U = 1{\cdot}22$ m/s, (*d*) $U = 1{\cdot}83$ m/s.

wave profiles at most 0·076 m apart. The wave patterns measured manually and automatically matched together quite well. The accuracy of measurements was probably better than $\pm 0{\cdot}5$ mm using the automated system, and about ± 1 mm using the manually set pointers.

Known lengths of run were timed automatically to measure the actual run speeds, which were on average about 0·3 % lower than the nominal values, and repeated within 1 %. Small speed differences between successive runs resulted in noticeable phase shifts and amplitude variations. These were largely eliminated from the bow wave by making all quantities dimensionless. Measured wave

heights and distances from the bow were multiplied by the transverse wave-number g/U^2 for each run, where g is the acceleration due to gravity and U the actual run speed. Small phase shifts in the shoulder wave could not be eliminated.

Figure 2 shows contour maps of the dimensionless wave height $g\zeta/U^2$ in the bow wave region with the model running at both speeds in each direction. The measured wave height was ζ, and the distances x and y were measured upstream from the craft bow and at right angles to the model centre-line respectively. The bow wave systems are clearly shown. In figure 2(*a*) the shoulder starts downstream at $gx/U^2 = -26{\cdot}2$, while in figures 2(*b*) and (*c*) it starts at

$$gx/U^2 = -11{\cdot}6 \quad \text{and} \quad -11{\cdot}8$$

respectively, so that the first trough of the shoulder wave just appears in the region shown. In figure 2(*d*) the forward wedge extends only to $gx/U^2 = -5{\cdot}2$, and the pattern is complicated by interference between the second bow wave crest and the first shoulder wave trough. Irregularities in the contour lines are probably mainly due to experimental inaccuracies, which were most serious at the slower speed and with the finer bow. Linear theory predicts some irregularities even when the model is as simple as a uniform source sheet (Jinnaka 1957) and certainly for a ship-shaped model (Mori *et al.* 1972).

3. Linear theory and numerical method

The double-wedge model described in § 2 is represented by a source distribution on the vertical centre-plane. The forward wedge is represented by a uniform panel of sources and the rear wedge by a uniform panel of sinks. The curved mid-section is ignored, being replaced by a mean straight section represented by a panel with zero source density. The model has zero total source strength. Jinnaka (1957) calculated the linear wave pattern set up by an infinitely deep uniform vertical sheet of wave-making sources in a uniform stream. Jinnaka's results are modified for a source sheet of finite depth.

The co-ordinate system is chosen to move with velocity U relative to the undisturbed fluid, with z measured vertically upwards from the undisturbed free surface, x measured upstream and y at right-angles to x and z. A wedge with side walls defined by $y = \pm x\tan\alpha$ extends downstream from the origin to $x = -l$, and from the free surface down to $z = -h$. If α is small, linear wave theory shows that the wedge may be modelled by a uniform source panel with density $U\tan\alpha/2\pi$ on the plane $y = 0$, extending from $x = 0$ to $x = -l$ and from $z = 0$ to $z = -h$.

An expression for the wave height due to a single wave-making source, quoted by Gadd (1969, equation (2)), was integrated over the source panel. The resulting linear wave height ζ at the point (x, y) due to the panel of sources is given by

$$\frac{g\zeta(x,y)}{U^2} = \frac{\tan\alpha}{\pi}\left\{\frac{1}{\pi}\int_{-\frac{1}{2}\pi}^{\frac{1}{2}\pi} d\theta \int_0^\infty \frac{K^*(1-e^{-Kh})}{K(K-K^*)}\left[\cos K(\overline{\omega}+l\cos\theta) - \cos(K\overline{\omega})\right] dK \right.$$
$$\left. + \int_{-\frac{1}{2}\pi}^{\frac{1}{2}\pi} (1-e^{-K^*h})\left[\sin K^*(\overline{\omega}+l\cos\theta) - \sin(K^*\overline{\omega})\right] d\theta\right\}, \qquad (1)$$

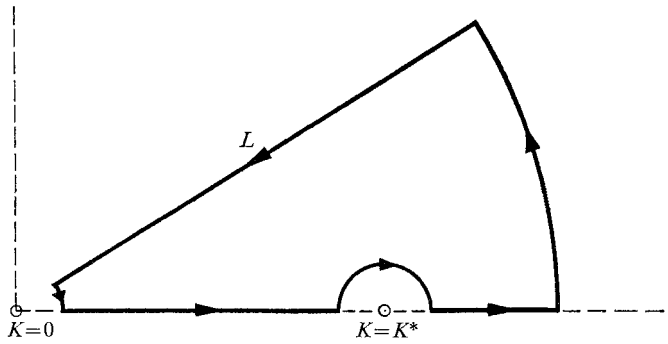

FIGURE 3. Contour of integration in the complex-K plane.

where $K^* = g\sec^2\theta/U^2$, $y \geqslant 0$, $\bar{\omega} = x\cos\theta + y\sin\theta$ and the principal value of the infinite K-integral is taken. Equation (1) may be split into four components:

$$\frac{g\zeta(x,y)}{U^2} = \frac{\tan\alpha}{\pi}\{Z(x,y,0) - Z(x,y,h) - Z(x+l,y,0) + Z(x+l,y,h)\}, \tag{2}$$

where

$$Z(x,y,h) = \frac{1}{\pi}\int_{-\frac{1}{2}\pi}^{\frac{1}{2}\pi} d\theta \int_0^\infty \frac{K^* e^{-Kh}}{K(K-K^*)}[1-\cos(K\bar{\omega})]\,dK - \int_{-\frac{1}{2}\pi}^{\frac{1}{2}\pi} e^{-K^*h}\sin(K^*\bar{\omega})\,d\theta$$

and the principal value is again taken.

The double integral is inconvenient to evaluate numerically because its integrand contains a pole at $K = K^*$, converges slowly when h is small and oscillates rapidly when $\bar{\omega}$ is large. To make the integration process both simple and rapidly convergent the infinite integral is re-expressed as part of a contour integral. A contour of integration in the complex-K plane is chosen away from the singularity at $K = K^*$, so that the integrand decays within one wavelength of the oscillatory part. A similar device has been used by others, including Wigley (1949) and Yeung (1972), with ϵ, defined below, set equal to zero. The reason for choosing non-zero ϵ will be explained later.

Figure 3 shows a typical integration contour. When $h = 0$ the line L is taken to be $K = iu$, where the new variable u is real and positive. The infinite integral in (2) is rewritten as

$$\mathrm{Re}\left\{\int_0^\infty \frac{K^*(1-e^{iK|\bar{\omega}|})}{K(K-K^*)}\,dK\right\} = K^{*2}\int_0^\infty \frac{e^{-u|\bar{\omega}|}-1}{u(u^2+K^{*2})}\,du + \pi\sin(K^*|\bar{\omega}|), \tag{3}$$

where $|\bar{\omega}|$, the absolute value of $\bar{\omega}$, is used to make the exponential term decay as $u \to \infty$. When $h > 0$, the infinite integral in (2) is split into two parts:

$$\mathrm{Re}\left\{\int_0^\infty \frac{K^* e^{-Kh}}{K(K-K^*)}\,dK - \int_0^\infty \frac{K^* e^{-Kh+iK|\bar{\omega}|}}{K(K-K^*)}\,dK\right\}. \tag{4}$$

These two integrals are re-expressed separately as parts of contour integrals. The line L in figure 3 now represents $K = u(1+i)/h$ for the first integral and

$K = u(1+i\epsilon)/(h-i|\overline{\omega}|)$ for the second, where the new variable of integration u and the constant ϵ are real and positive on L. Equation (4) is rewritten as

$$\int_0^\infty \frac{K^* e^{-Kh}}{K(K-K^*)}(1-\cos K\overline{\omega})\,dK$$
$$= K^{*2}\int_0^\infty \left\{\frac{f_2}{u^2-K^*uh+\frac{1}{2}K^{*2}h^2}-\frac{f_1}{u^2-2K^*up_r+K^{*2}|p|^2}\right\}$$
$$\times\frac{e^{-u}}{u}\,du+\log[h/2^{\frac{1}{2}}|p|], \qquad (5)$$

where
$$p = p_r+ip_i = (h-i|\overline{\omega}|)/(1+i\epsilon), \quad |p| = (p_r^2+p_i^2)^{\frac{1}{2}},$$
$$f_1 = (up_r/K^*-|p|^2)\cos(\epsilon u)+(up_i/K^*)\sin(\epsilon u),$$
$$f_2 = \tfrac{1}{2}\{(uh/K^*-h^2)\cos u-(uh/K^*)\sin u\}.$$

Thus Z in (2) is given by

$$Z(x,y,0)-Z(x,y,h) = \frac{1}{\pi}\int_{-\frac{1}{2}\pi}^{\frac{1}{2}\pi} d\theta\int_0^\infty \left\{\frac{e^{-u|\overline{\omega}|}-1}{Q^2u^2+1}\right.$$
$$\left.+\frac{f_1e^{-u}}{Q^2u^2-2Qup_r+|p|^2}-\frac{f_2e^{-u}}{Q^2u^2-Quh+\frac{1}{2}h^2}\right\}\frac{du}{u}$$
$$-\frac{1}{\pi}\int_{-\frac{1}{2}\pi}^{\frac{1}{2}\pi}\log[h/2^{\frac{1}{2}}|p|]\,d\theta-2\int_{-\frac{1}{2}\pi}^{\theta'}(1-e^{-K^*h})\sin(K^*\overline{\omega})\,d\theta, \qquad (6)$$

where $Q = (U^2\cos^2\theta)/g$, $\theta' = \tan^{-1}(-x/y)$ with $-\frac{1}{2}\pi \leqslant \theta' \leqslant \frac{1}{2}\pi$, and other quantities are defined under (1) and (5).

If $\epsilon = 0$, as in earlier papers, the line L in figure 3 approaches $K = K^*$ as $|\overline{\omega}|/h$ becomes small, and the integrand on L develops a sharp peak and trough. Yeung (1972) overcame this problem by making a complicated series expansion of the integrand near $K = K^*$. A more simple device is merely to choose a suitable non-zero ϵ. The integrand involving f_1 and f_2 decays as e^{-u} and oscillates as $\cos\epsilon u$, and so decays within one wavelength when $|\epsilon| < 1$. A suitable value is $\epsilon = \exp(-|\overline{\omega}|/h)$ for $h > 0$. This keeps the line L well clear of the singularity at $K = K^*$.

The infinite u-integral in $Z(x,y,0)$ was written in terms of known functions:

$$\int_0^\infty \frac{(e^{-u|\overline{\omega}|}-1)}{(Q^2u^2+1)}\frac{du}{u}\left\{\begin{array}{ll} = -\gamma-\log\eta-g(\eta) & \text{for} \quad \eta \neq 0, \\ = 0 \quad \text{when} & \eta = 0, \end{array}\right\} \qquad (7)$$

where $\eta = |\overline{\omega}|/Q$, $g(\eta)$ is defined by Abramowitz & Stegun (1965, equation 5.2.7) in terms of sine and cosine integrals,

$$g(\eta) = -\mathrm{Ci}\,\eta\cos\eta-\mathrm{si}\,\eta\sin\eta,$$

and $\gamma = 0{\cdot}5772156649\ldots$ is Euler's constant. The function $g(\eta)$ was calculated using Abramowitz & Stegun's rational approximation (5.2.39) for large η, and a polynomial approximation to $g(\eta)+\log\eta$ for small η.

The singularity in the remaining u-integral part of $Z(x,y,h)$ at $u = 0$ was removed by writing

$$\int_0^\infty [\cos u-\cos(\epsilon u)]\frac{e^{-u}}{u}\,du = \tfrac{1}{2}\log\left(\frac{1+\epsilon^2}{2}\right), \qquad (8)$$

when the integrals involving f_1 and f_2 give

$$\int_0^\infty \left\{\frac{f_1}{Q^2u^2-2Qup_r+|p|^2}-\frac{f_2}{Q^2u^2-Quh+\frac{1}{2}h^2}\right\}\frac{e^{-u}}{u}\,du$$
$$=\tfrac{1}{2}\log\frac{1+\epsilon^2}{2}+\int_0^\infty\left\{\frac{(Qu-p_r)\cos(\epsilon u)+p_i\sin(\epsilon u)}{Q^2u^2-2Qup_r+|p|^2}\right.$$
$$\left.-\frac{(Qu-\frac{1}{2}h)\cos u-\frac{1}{2}h\sin u}{Q^2u^2-Quh+\frac{1}{2}h^2}\right\}Q\,e^{-u}\,du. \qquad (9)$$

Since the integrals in (9) contain no singularities and decay within one wavelength, the numerical integration process was straightforward. The trapezium rule was used. Integration steps $\delta u = 0{\cdot}5$ between $u = 0$ and $u = 4{\cdot}5$ gave sufficient accuracy at the chosen wedge depth h. Then steps $\delta\theta = \frac{1}{10}\pi$ were sufficient to integrate (9) with respect to θ. Evaluation of the integral in $\log\eta + g(\eta)$ involved the substitution $t = \tan\theta$, suggested by Jinnaka (1957), and required three integration ranges, the step length increasing away from $t = \tan\theta'$. The last single integral in (6) shows pathological oscillations at $\theta = \pm\frac{1}{2}\pi$. The substitution $t = \tan\theta$ made the integrand decay fast enough for numerical computation. The rules for choosing step lengths δt and integration ranges for t were complicated, depending on θ', x and y, but were explained by Jinnaka.

In this way (2) was evaluated for source and sink panels describing the double-wedge model. The single-integral free-wave contribution to $Z(x,y,h)$ was negligible compared with $Z(x,y,0)$ at the model speeds and draught chosen. But the double-integral local contributions to $Z(x,y,h)$ and $Z(x,y,0)$ were of comparable size, and the model cannot be considered of infinite draught. Far upstream

$$Z(x,y,0)\sim\frac{1}{\pi}\int_{-\frac{1}{2}\pi}^{\frac{1}{2}\pi}[-\gamma-\log\eta-g(\eta)]\,d\theta$$
$$\sim -\gamma-\log(2gr/U^2)+O(U^2/gr)\text{ for large } r,$$

where $r^2 = x^2+y^2$ and Abramowitz & Stegun's (1965) equations (4.3.145) and (5.2.30) have been used. Thus when r is large, but within a few panel lengths l,

$$Z(x,y,0)-Z(x+l,y,0)\sim\tfrac{1}{2}\log[(r^2+l^2+2xl)/r^2] \qquad (10)$$

upstream. Although this is reduced by finite draught contributions, the local disturbance dies away slowly, and the source panels have considerable upstream influence. Thus the forward wedge cannot be considered of infinite length in describing the bow wave. The finite draught and length contributions all vary slowly along the model, and represent a general lowering of the water level around the bow rather than a change in the phase pattern.

Many lengths l upstream the behaviour of (10) becomes algebraic rather than logarithmic. When r is large compared with both length and draught, the panel behaves as a wave-making point source, for which Peters, quoted by Ursell (1960), found an upstream decay of wave height as $O(1/r^3)$.

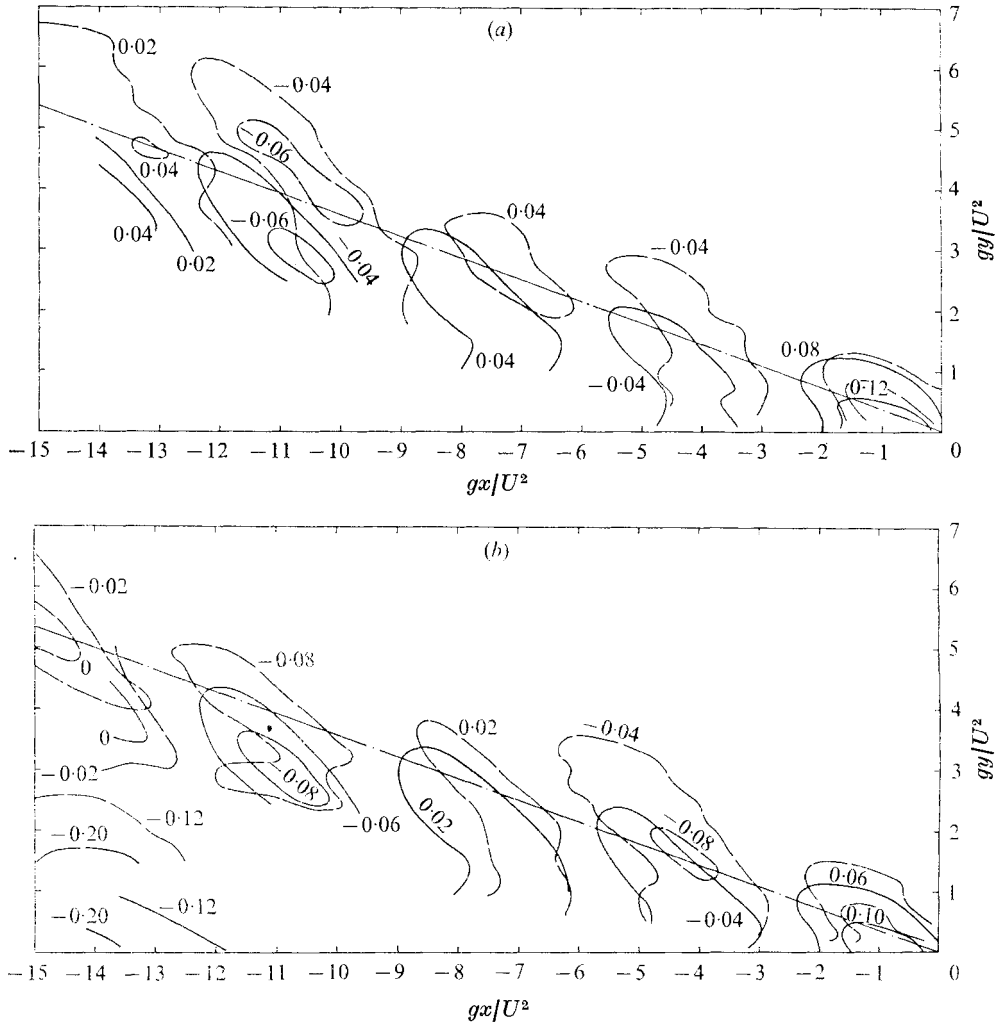

FIGURES 4(*a*, *b*). For legend see facing page.

4. Linear theory and experiment

Figure 4 compares contours of the dimensionless bow wave height $g\zeta/U^2$ predicted by linear theory with measured contours taken from figure 2. Both patterns show similar features, but while the calculated wave crests and troughs all lie within the critical line, the corresponding measured bow waves lie well outside. The outward phase shift starts at the bow with the first wave crest, and persists downstream, at least to the shoulder. At the higher speed the shift seems to be roughly constant after the first crest, but at the lower speed successive crests and troughs appear further outboard of the predicted pattern. The shift is larger around the blunter bow and is roughly proportional to the bow wedge angle.

Rather better agreement is obtained by rotating the theoretical pattern through

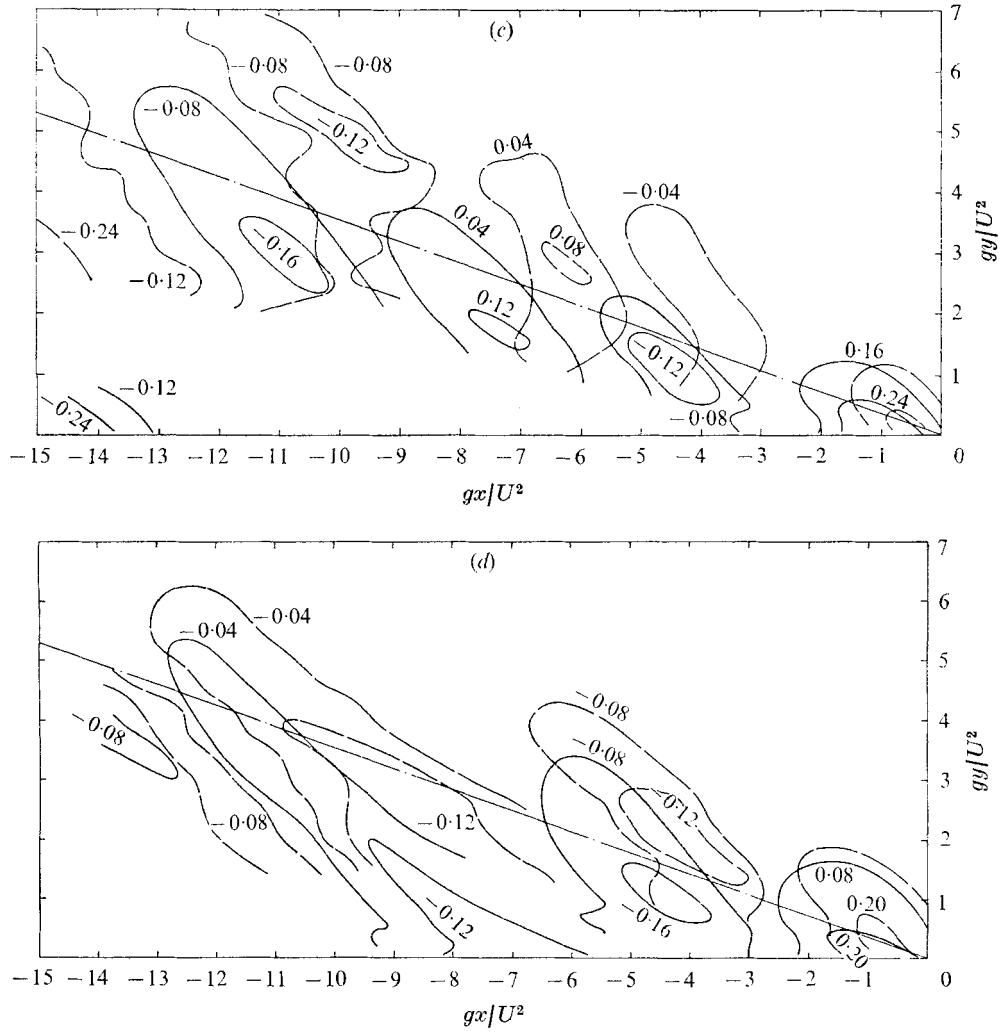

FIGURE 4. Contour maps of measured wave height $g\zeta/U^2$ compared with linear theory. The numbers indicate the dimensionless contour heights. Cases (*a*), (*b*), (*c*) and (*d*) as in figure 2. ———, linear theory; — — —, experiment; —·—, critical line at angle 19° 28′ to x axis.

the wedge half-angle about the bow, making the centre-plane boundary of the linear flow coincide with the actual bow wedge wall. The rotation does not shift the first wave crest far enough outwards, and moves following crests and troughs too far. This kind of improvement may be expected if the phase shift occurs because waves ride on the deflected flow parallel to the wedge wall. But Gadd (1970) showed that no such improvement is expected if the wave-making sources are merely split in two and shifted onto the wedge walls, while the basic flow remains parallel to the centre-plane. The basic flow itself must be deflected.

Figure 5 compares profiles of measured and linear wave height at points along the side of the model. The measured profiles show a forward phase shift,

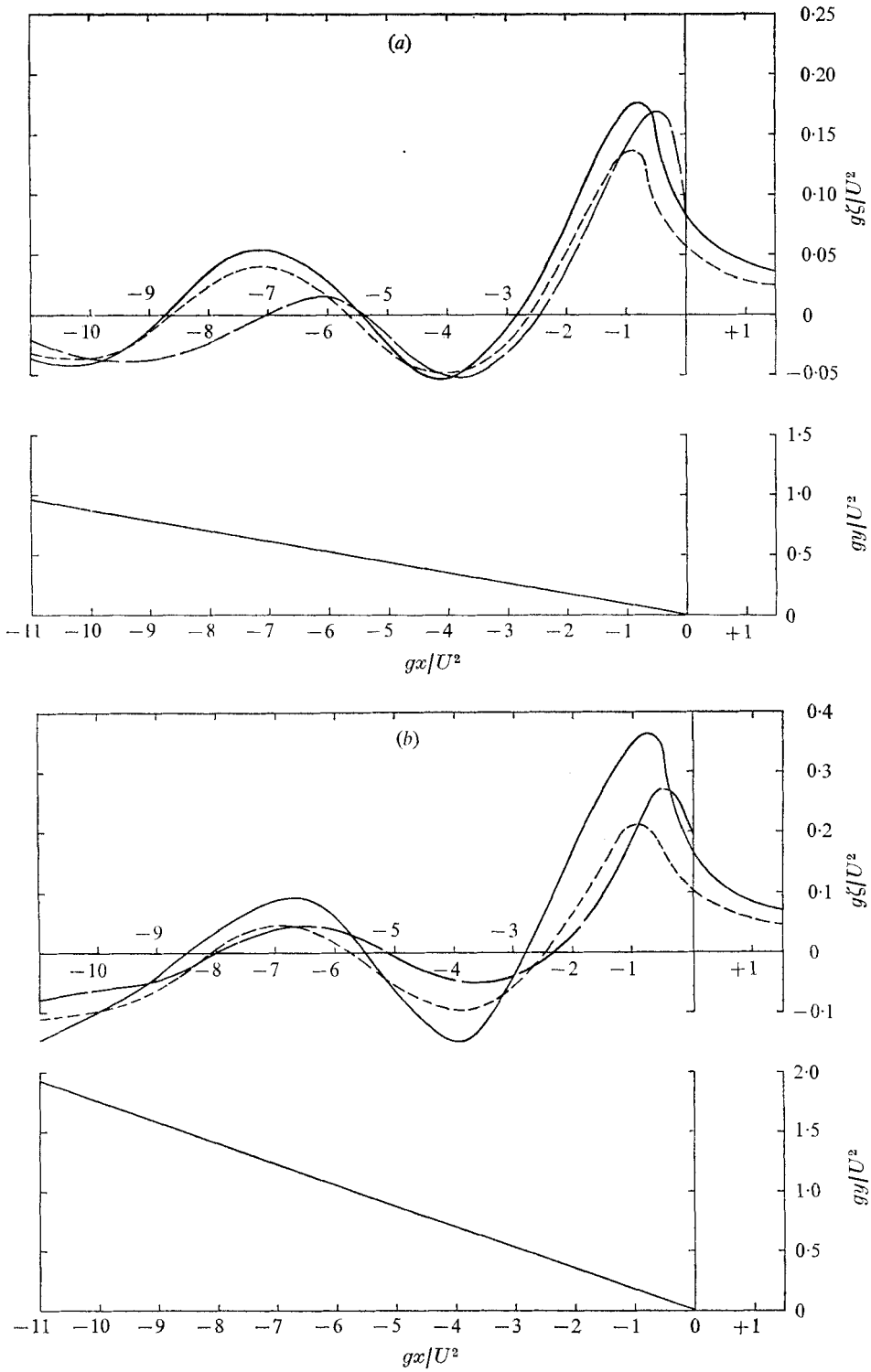

FIGURE 5. Profiles of wave height $g\zeta/U^2$ along the hull surface. The surface streamline is shown below each profile. U = 1·22 m/s. (*a*) Fine bow. (*b*) Blunt bow. ———, linear theory; — — —, experiment; - - - - - -, Guilloton's method.

and the first crest is steeper than predicted, but has roughly the right amplitude. Nonlinear steepness effects, resulting in increased phase velocities, are probably most important at the first crest. Downstream of this crest linear theory predicts steeper waves than were measured, with more pronounced crests and troughs.

In this connexion recent work, in particular of Reed & Ursell, presented to the *Workshop on Slender Body Theory* at Michigan, suggests that the rate of decay of ship-generated waves along the side of a long ship is greater than linear theory predicts, and that this may be due to the refraction of the waves by the side of the ship itself.

5. The Guilloton transformation

Using an intuitive physical approach Guilloton (1964) proposed the following method for estimating the effects of nonlinearities in the free-surface and hull-surface conditions. The linearized solution is valid only when the hull is thin, the flow velocity is almost uniform and the streamlines almost horizontal and parallel to the hull centre-plane. On a real hull the velocity is decreased near the bow and stern and increased amidships, and fluid particles have to travel a distance increased by the local streamline slope. Guilloton related points in a so-called 'real' space to points in a 'linearized' space, the 'real' points being displaced in all three co-ordinate directions relative to the corresponding 'linearized' points as discussed below. He proposed that particles would take the same time to travel between two points along a streamline in the 'real' flow as between corresponding points in the undisturbed uniform flow, where the speed of 'real' particles along streamlines is obtained from the linear solution at corresponding points. Guilloton showed that the resulting 'real' solution closely satisfies the Laplace equation and boundary conditions, assuming that the streamlines are close to isobars. Guilloton made up his linearized hull from wedges, equivalent to source panels as in § 3. The source strengths were calculated to make the centre-plane of the 'linearized' hull correspond to the surface of the 'real' hull.

Emerson (1971) and Gadd (1973) applied Guilloton's method to calculations of hull surface wave profiles and wave-making resistance for mathematical and ship models. The wave profiles showed a forward phase shift and smoothing out of wave crests and troughs to bring them and the resulting wave-resistance curves into close agreement with experiment. Guilloton's method is used here to calculate wave profiles along streamlines near the double-wedge model.

Co-ordinates (x_0, y_0, z_0) and (x, y, z) are taken in the 'linearized' and 'real' spaces respectively. The linearized hull is modelled by an array of point sources on the centre-plane $y_0 = 0$, except that, where flow velocities are required on the centre-plane itself, each source is assumed to be spread over a panel. The undisturbed uniform flow velocity is U in the negative x_0 direction and the linearized flow velocity, when disturbed by the source array, is $(u_0 - U, v_0, w_0)$ at the point (x_0, y_0, z_0). This point transforms into the 'real' point (x, y, z) according to

$$x = x_0 + \xi, \quad y = y_0 + \eta, \quad z = z_0 + \zeta, \tag{11}$$

where $$d\eta/dx_0 = -v_0/U, \quad d\xi/dx_0 = q/[U(1+\tfrac{1}{2}\alpha^2)] - 1,$$
$$\zeta = (U^2 - q^2)/2g,$$

q is the flow speed at (x_0, y_0, z_0),

$$q^2 = (u_0 - U)^2 + v_0^2 + w_0^2$$

and α is the angle between the 'real' streamline and the x axis, which is approximately the angle between the linearized streamline and the x_0 axis,

$$\alpha \simeq (v_0^2 + w_0^2)^{\frac{1}{2}}/U.$$

The linear velocity components u_0, v_0 and w_0 were obtained by differentiating the velocity potential due to a source, quoted by Gadd (1969, equation (1)). At the free surface $z_0 = 0$ the velocity components due to a single source of strength m at depth $z_0 = -\bar{Z}$, where $\bar{Z} > 0$, are

$$[u_0, v_0, w_0]_{z_0=0} = \frac{2m}{\pi}\int_{-\frac{1}{2}\pi}^{\frac{1}{2}\pi} d\theta \int_0^\infty \frac{\mathbf{A}}{K - K^*} e^{-K\bar{z}} K\, dK + 2m \int_{-\frac{1}{2}\pi}^{\frac{1}{2}\pi} \mathbf{B}\, e^{-K^*\bar{z}} K^{*2} d\theta, \tag{12}$$

where

$$\mathbf{A} = [-K^* \cos\theta \sin(K\bar{\omega}_0), -K^* \sin\theta \sin(K\bar{\omega}_0), K\cos(K\bar{\omega}_0)],$$
$$\mathbf{B} = [\cos\theta \cos(K^*\bar{\omega}_0), \sin\theta \cos(K^*\bar{\omega}_0), \sin(K^*\bar{\omega}_0)],$$
$$K^* = g\sec^2\theta/U^2, \quad \bar{\omega}_0 = x_0 \cos\theta + y_0 \sin\theta.$$

Equations (12) were re-expressed in terms of contour integrals as in §3. The contour in the complex-K plane is shown in figure 3. The line L now represents $K = u(1 + i\epsilon)/(\bar{Z} - i|\bar{\omega}_0|)$, where the new integration variable u and constant ϵ are real and positive. The new integrand decays as e^{-u} and oscillates as $\cos(\epsilon u)$, so that the numerical integration process is most efficient when $|\epsilon| < 1$. Choosing $\epsilon = \exp(-|\bar{\omega}_0|/\bar{Z})$ keeps the line L clear of the singularity at $K = K^*$, and the integrand decays within one wavelength. The resulting integrals, similar to (6), were evaluated using the trapezium rule.

The centre-plane source array was found iteratively, the first approximation being an array of Michell sources proportional to the local water-line slopes. The source strengths were adjusted until the plane $y_0 = 0$ transformed into the hull surface $y = \eta_0(x, z)$. Then equations (11) gave the wave elevation $\zeta(x, y)$ along the surface water-line by transforming points on the line $y_0 = 0$, $z_0 = 0$. To evaluate wave heights away from the hull surface it was assumed that far upstream the flow is uniform, and a transverse plane $x_0 = a_0$ transforms into another transverse plane $x = a$, where a_0 and a are constants. Then starting from a point $(a_0, b_0, 0)$ on the linearized plane, surface elevations $\zeta(x, b)$ were calculated at successive downstream points by transforming the line $y_0 = b_0$, $z_0 = 0$ according to (11).

As these calculations were expensive in terms of computing time, wave profiles were calculated along four lines only, corresponding to $gy_0/U^2 = 0$, 1, 2 and 3·5, with the model running in each direction at the two nominal speeds. Figures 5 and 6 show Guilloton wave profiles for the first two cases at the lower speed. Below each profile is the Guilloton streamline in the x, y plane, the transform of

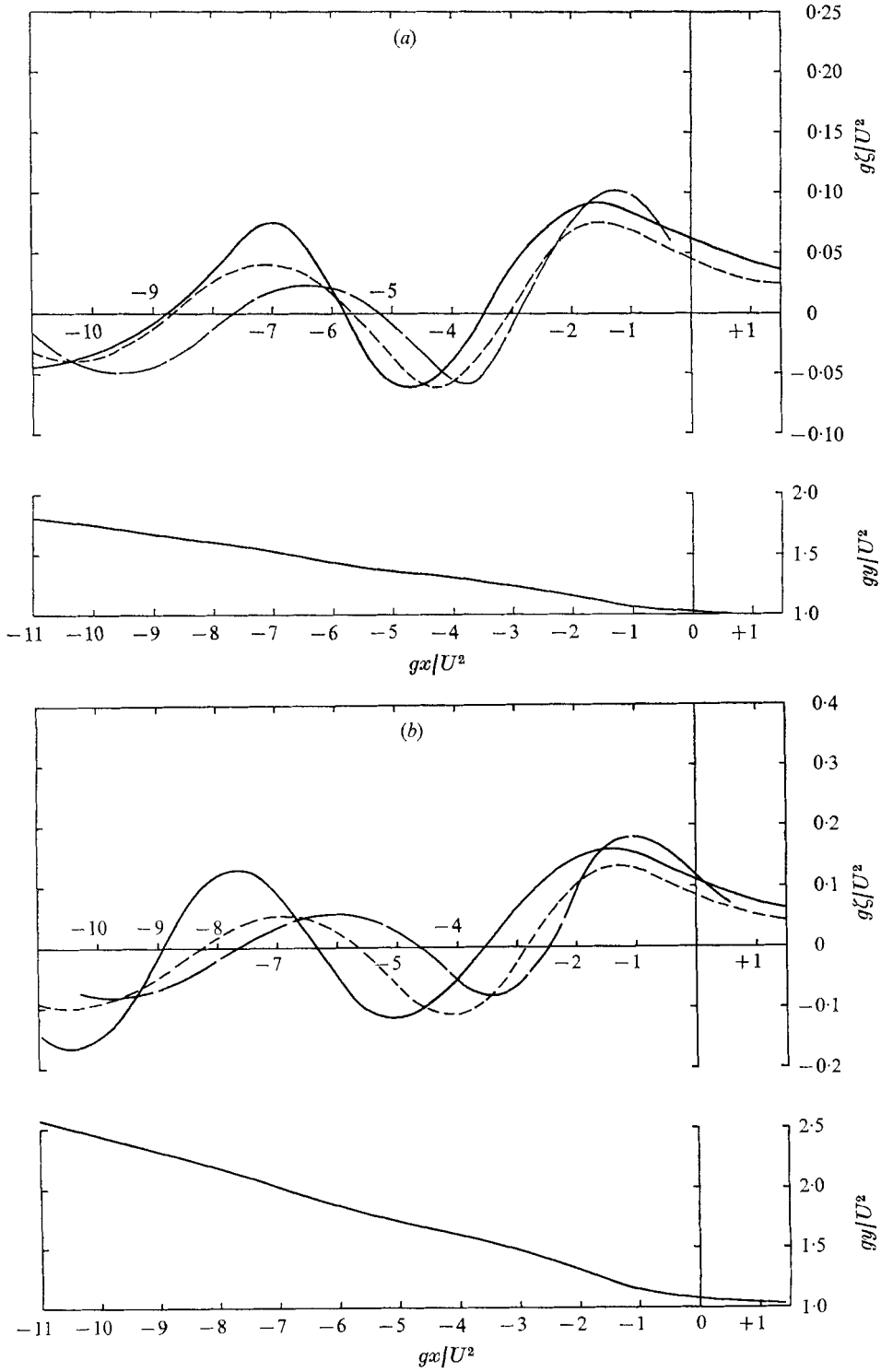

FIGURE 6. Profiles of wave height $g\zeta/U^2$ along the Guilloton transforms of $gy_0/U^2 = 1$. Notation as in figure 5.

the appropriate straight line. Also shown are wave profiles along the same 'streamlines' taken from the experimental maps in figure 2 and calculated using linear theory. The Guilloton profiles show forward phase shifts relative to the linear profiles, but these are generally less than half those of the experimental profiles, and decrease away from the model. In contrast the experimental profiles show, if anything, increasing shifts away from the model. In all cases the first crest at the bow was steeper than either theory predicts, but linear theory predicts its amplitude better. The remainder of the wave train was smoothed out, so that the Guilloton wave profiles look generally more realistic than the linear ones. In particular the trough following the first crest is predicted by Guilloton's method to be shallower than the corresponding linear trough.

6. Conclusions

The measured wave pattern set up by a deep wedge-ended model generally resembled the calculated linear pattern, but there were several consistent differences.

(i) The measured pattern showed an outward phase shift, with crests and troughs lying well outside the theoretical critical line.

(ii) At the higher speed the shift was roughly constant after the first crest, but at the lower speed successive crests and troughs showed further outward shifts.

(iii) The shift was roughly proportional to the bow wedge half-angle. Rotating the linear pattern about the bow through this angle reduced the phase discrepancies, but did not shift the first crest far enough, and shifted following crests and troughs too far outboard. No such improvement is expected if wave-making sources are merely placed on the model walls, the basic flow being undeflected.

(iv) The first crest at the bow had roughly the right amplitude, but was steeper than linear theory predicted.

(v) Following crests and troughs were less pronounced than linear theory predicted. The smoothing-out process may involve the refraction of waves outwards by the model wall.

Guilloton's method attempts to estimate the effects of nonlinearities in the hull- and free-surface conditions.

(i) Compared with linear theory the Guilloton profiles were in better phase agreement with the measured profiles. They showed about half the measured phase shift close to the model, but rather less further away.

(ii) The amplitude of the first wave crest at the bow was predicted better by linear theory.

(iii) The following wave system, in particular the first trough, was smoothed out, so that the Guilloton wave profiles looked generally more realistic than the linear profiles.

These results confirm Gadd's (1973) conclusion that the Guilloton method seems to predict the wave pattern rather better than linear theory. But the improvements were generally less impressive than Gadd's, and much of the

far-field phase shift remains unexplained. Guilloton's method is hard to justify theoretically. His solution seems to satisfy the hull- and free-surface conditions more accurately than the linear solution, but does not satisfy the Laplace equation exactly. Guilloton showed that in the two-dimensional case his method predicts trochoidal waves (Lamb 1932, § 251). These waves, although rotational, satisfy the free-surface condition exactly. They steepen realistically at the crests and flatten out in the troughs, but their speed is independent of wave amplitude, and so they are in phase with linear waves. Thus Guilloton's ship-wave profiles probably have a more realistic shape than linear ones, but their phase is unlikely to change much with wave steepness.

The effects of wave steepness on the pattern may perhaps be estimated by comparison with Hogben's (1972*a*) results for the nonlinear interacting free-wave system set up by a single Kelvin source. Neglecting local terms, Hogben calculated the third-order free-wave crest envelopes in a channel of finite width. For comparison with the double-wedge model a representative wave steepness was taken to be the difference in wave height between the first crest and the following trough divided by the horizontal crest-to-trough distance. The strength of the corresponding single source was chosen to make this free-wave steepness for source and model the same. At the lower model speed Hogben's Froude number F_b was 0·158. Comparable single source results were not available, but the wave steepnesses, and thus presumably any phase effects, were similar to those at the higher model speed, with $F_b = 0{\cdot}237$. At that speed, taking Hogben's source depth parameter Z to be 0·025 or 0·05, his source strength parameter Q was found to be 6×10^{-4} or $1{\cdot}5 \times 10^{-3}$ respectively with the fine bow, and $1{\cdot}2 \times 10^{-3}$ or 3×10^{-3} respectively with the blunt bow. At $F_b = 0{\cdot}25$ Hogben showed that phase shifts are small when $Q = 0{\cdot}01$ and 0·02, and decrease rapidly with Q. Thus the observed shifts are unlikely to be the result of interactions in the free-wave system alone.

Instead they may be caused by the local wave component interacting with the free wave. This may steepen the wave enough to affect its speed locally near the bow. But at the same time the free waves ride outwards on the mean local flow deflected around the hull. It is hard to assess the relative importance of these two effects. Both depend on the local term, which, while finite length and depth effects remain, increasingly steepens and convects outwards the bow wave as the craft speed is reduced. This trend was noted in the measured wave patterns. Guilloton's method probably describes convection shifts fairly well. A theoretically more justifiable approach was suggested by Dagan (1972), and further study along those lines is in hand. At present there are no reliable estimates of wave steepness effects at the bow.

The author wishes to thank Dr G. E. Gadd for help and advice during the preparation of this paper.

REFERENCES

ABRAMOWITZ, M. & STEGUN, I. A. 1965 *Handbook of Mathematical Functions*. Dover.

DAGAN, G. 1972 *Proc. 9th ONR Symp. on Naval Hydrodyn., Paris*, to appear.

EGGERS, K. W. H. 1970 *Stevens Inst. Tech., Davidson Lab. Rep.* SIT-DL-70-1423.

EMERSON, A. 1971 *Trans. N.E. Coast Instn. Engrs Shipb.* **87**, 139.

EVEREST, J. T. & HOGBEN, N. 1970 *Trans. Roy. Instn. Nav. Archit.* **112**, 319.

GADD, G. E. 1969 *Trans. Roy. Instn. Nav. Archit.* **111**, 487.

GADD, G. E. 1970 *Trans. Roy. Instn. Nav. Archit.* **112**, 335.

GADD, G. E. 1971 *Nat. Phys. Lab. Ship Rep.* no. 156.

GADD, G. E. 1973 *Trans. Roy. Instn. Nav. Archit.* to appear.

GUILLOTON, R. 1964 *Bull. Ass. Tech. Maritime & Aeronautique*, **64**, 537.

HOGBEN, N. 1957 *Trans. Roy. Instn. Nav. Archit.* **99**, 446.

HOGBEN, N. 1971 *Trans. Roy. Instn. Nav. Archit.* **113**, 345.

HOGBEN, N. 1972*a* *J. Fluid Mech.* **55**, 513.

HOGBEN, N. 1972*b* *Trans. Roy. Instn. Nav. Archit.* **114**, 127.

HOVGAARD, W. 1909 *Trans. Roy. Instn. Nav. Archit.* **51**, 251.

INUI, T. 1962 *Trans. Soc. Nav. Archit. Mar. Engrs*, **70**, 283.

JINNAKA, T. 1957 *Soc. Nav. Archit. Japan, 60th Anniv. Ser.* **2**, 83.

KAJITANI, H. 1963 *Proc. Int. Seminar Theoretical Wave Resistance*. Ann Arbor.

LAMB, H. 1932 *Hydrodynamics*, 6th edn. Cambridge University Press.

MORI, K., INUI, T. & KAJITANI, H. 1972 *Proc. 9th ONR Symp. Naval Hydrodyn., Paris*, to appear.

NEWMAN, J. N. 1971 *J. Ship Res.* **15**, 1.

SHEARER, J. R. 1951 *Trans. N.E. Coast Instn. Engrs Shipb.* **67**, 43.

URSELL, F. 1960 *J. Fluid Mech.* **8**, 418.

VAN DYKE, M. 1964 *Perturbation Methods in Fluid Mechanics*. Academic.

WIGLEY, W. C. S. 1931 *Trans. N.E. Coast Instn. Engrs Shipb.* **47**, 153.

WIGLEY, W. C. S. 1949 *Bull. Ass. Tech. Maritime & Aeronautique*, **48**, 533.

YEUNG, R. W. 1972 *J. Ship Res.* **16**, 47.

YIM, B. 1964 *Hydronautics Inc. Tech. Rep.* no. 117–5.